

1 **Response of modern fluvial sediments to regional tectonic activity**
2 **along the upper Min River, Eastern Tibet**

3
4 Wei Shi^{1,2}, Hanchao Jiang^{1,2,*}, Hongyan Xu^{1,2}, Siyuan Ma¹, Jiawei Fan^{1,2}, Siqi
5 Zhang¹, Qiaoqiao Guo¹, Xiaotong Wei¹

6
7 *¹State Key Laboratory of Earthquake Dynamics, Institute of Geology, China*
8 *Earthquake Administration, Beijing 100029, China*

9 *²Lhasa Geophysical National Observation and Research Station, Institute of Geology,*
10 *China Earthquake Administration, Beijing 100029, China*

11
12 **Corresponding author:** Hanchao Jiang, E-mail: hcjiang@ies.ac.cn

13

14 **Abstract**

15 The deposition of fluvial sediments in tectonically active areas is mainly controlled
16 by tectonics, climate, and associated Earth surface processes; consequently, fluvial
17 sediments can provide a valuable record of changes in regional climate and tectonic
18 activity. In this study, we conducted a detailed analysis of the grain-size distribution in
19 modern fluvial sediments from the upper Min River, Eastern Tibet. These data, ~~were~~
20 combined with ~~regional~~ information ~~about of regional~~ climate, vegetation, hydrology,
21 geomorphology, lithology, and fault slip rate, ~~and together~~ indicate that modern regional
22 tectonic activity along upper Min River can be divided into three segments. Specifically,
23 fluvial sediments in the segment I are dominated by ~~fine~~-silts (<63 μm : ~~70.2%~~),
24 agreeing with a low-runoff ~~and~~ low-rainfall ~~and high vegetation cover in this segment~~
25 and revealing a windblown origin influenced by the arid and windy climate. These
26 observations are consistent with the ~~segment's~~ low hillslope angle and low relief ~~in~~
27 ~~segment I~~, all indicating weak activity along the Minjiang Fault. The coarse-grained
28 fraction (>250 μm) of fluvial sediments in the segments II ~~=and~~ III increases ~~in a~~
29 stepwise ~~fashion (A = 6.2%, B = 19.4%, C = 33.8%)~~ downstream, although runoff and
30 rainfall do not change significantly from segment II to segment III. These patterns
31 correlate well with ~~an~~ ~~increases~~ in both regional relief and hillslope angles. Together,
32 these observations imply that regional tectonic activity along Maoxian–Wenchuan Fault
33 becomes more pervasive downstream along the Min River. ~~Fluvial sediments in~~
34 ~~segment IV are well sorted and well rounded, which is expected due to significant~~
35 ~~increases in rainfall and runoff in this segment. The occurrence of well-sorted and well-~~

36 rounded pebbles of fluvial sediments in downstream of Dujiangyan must be related to
37 the long-time scouring and sorting by rivers. This study marks the first development of
38 a new and important research approach that can characterize regional tectonic activity
39 by analysis of grain-size distribution of fluvial sediments collected from tectonically
40 active regions, ~~combined with regional conditions in geology and geography.~~

41

42 **Keywords:** Modern fluvial sediments; Grain-size analysis; Tectonic activity; Upper

43 Min River; Eastern Tibetan Plateau

44

45 **1 Introduction**

46 Tectonic geomorphology is a relatively young sub-discipline of geomorphology,
47 and has the major aim of unraveling interactions between tectonic activity, climate, and
48 Earth surface processes (Wobus et al., 2005; Owen, 2013). The grain-size distribution
49 of river bed material, channel width, channel sinuosity, extent of alluvial cover,
50 lithology of bedrock, and hydraulic roughness are all potentially important variables
51 (Whipple, 2004; Whittaker et al., 2010). Thus, comprehensive amounts of data must be
52 collected in a wide range of field settings before the responses of these important
53 variables to climatic and tectonic forcings can be determined.

54 The topographic margin of the Tibetan Plateau (TP) along the Longmen Shan is
55 one of the most impressive continental escarpments in the world, and the land surface
56 rises westward over a horizontal distance of 40–60 km from the Sichuan Basin (500–
57 700 m elevation) to peak elevations exceeding 6000 m (Chen et al., 2000; Kirby et al.,
58 2000, 2008). Some studies have revealed common topographic features within river
59 channels in the eastern TP, namely, an upper low-gradient channel segment, a middle
60 steep-gradient channel segment, and a low-lying very steep channel segment, such as
61 in the Red River region in Yunnan Province (Schoenbohm et al., 2004) and the Min
62 River region in Sichuan Province (Kirby et al., 2003). However, it is important to note
63 that strong lithological contrasts along the length of a river can also cause the channel
64 steepness index to change at comparable magnitudes to those associated with large
65 gradients in rock uplift rate (Snyder et al. 2000; Stock and Dietrich 2003; Beek and
66 Bishop 2003; Whittaker et al., 2010). New data sourced from several localities record
67 an apparent narrowing of channel width in response to increased rock uplift rates in

68 rivers with large areas of bedrock (Whipple, 2004). This is consistent with the recent
69 proposition that river profiles straighten as aridity increase (Chen et al., 2019), as
70 observed along the upper Min River in the field. Generally, exposures of hard bedrock
71 often generate straight channels, which have low channel slopes and small sediment
72 loads (Schumm and Khan, 1971, 1972).

73 Vegetation density can modulate topographic responses to changing denudation
74 rates, such that the functional relationship between denudation rate and topographic
75 steepness becomes increasingly linear as vegetation density increases (Olen et al., 2016).
76 Recent studies indicate that the upper Min River has poor vegetation coverage and most
77 regions are fully exposed due to the strongly arid climate conditions (Jiang et al., 2015;
78 Xu et al., 2020; Shi et al., 2020; Wei et al., 2021; Zhou et al., 2021). Thus, hillslope
79 colluvium is the dominant sediment source to the upper Min River – especially in its
80 middle and lower segments (Zhang et al., 2021) – akin to those in drainage basins in
81 many arid regions worldwide (Clapp et al., 2002).

82 Tectonic activity influences the evolution of lacustrine sedimentary sequences by
83 affecting the provenance supply (Najman, 2006; Jiang et al., 2022). Frequent
84 earthquakes on the TP, as recorded by widely distributed soft sediment deformation
85 (Wang et al., 2011; Xu et al., 2015; Jiang et al., 2016; Zhong et al., 2019; Zhang et al.,
86 2021), caused repeated landslides that also represent another major source of sediment
87 into the upper Min River (Dai et al., 2011; Xu et al., 2012, 2013). These landslides
88 generated a large amount of dust storms that deposited dust in nearby lakes (Jiang et al.,
89 2014, 2017) and exposed large quantities of fine-grained sediment that had
90 accumulated on mountain slopes, which were subsequently transported by wind to
91 ancient lakes, documenting these seismic events (Whittaker et al., 2010; Liang and
92 Jiang, 2017; Shi et al., 2022). This sedimentological process was recently recognized at

93 Huojizhai, Diexi Town, following the historical earthquake at Diexi in 1933 (Wei et al.,
94 2021).

95 Changes in hydrology and sediment flux are commonly regarded as climate
96 forcing (Wobus et al., 2010). The extent of alluvial cover is very limited throughout the
97 upper Min River Basin, which is demonstrated by similarity of zircon U–Pb ages in
98 lacustrine sediments and their nearby bedrock units (Zhong et al., 2017). As such, the
99 influence of occasional flood events should be considered over long time–_scales
100 (Snyder and Whipple, 2003), as aridity precludes rainfall or fluvial undercutting as
101 being the trigger for such events.

102 The consistent climate coupled with systematic variations in lithology and rock
103 uplift rate along the Min Mountains allow comparison of channels that experience
104 different tectonic forcings (Duvall et al., 2004). Selective transport is the dominant
105 downstream fining mechanism in this region, although rates of selective transport in
106 sand–bed rivers are smaller than those in gravel–bed rivers (Frings, 2008).

107 Only a small volume of sediment collected from a river bed is needed to produce
108 a transformative understanding of the rates at which landscapes change (Blanckenburg,
109 2005). Study of these materials can reveal relationships between generation, transport
110 (Clapp et al., 2000, 2002), and mixing of sediment (Perg et al., 2003; Nichols et al.,
111 2005), under the help of the key topographic and/or lithologic features (e.g., relief, slope
112 angle, and substrate characteristics) (Riebe et al., 2000; Riebe et al., 2001; Matmon et
113 al., 2003a, b). In this study, we combine field ~~observations, surveys,~~ and analysis of
114 river sediments in the upper Min River to determine hydraulic characteristics, and
115 topographic and tectonic information about bedrock channels ~~in the upper Min River.~~

116

117 **2 Regional setting**

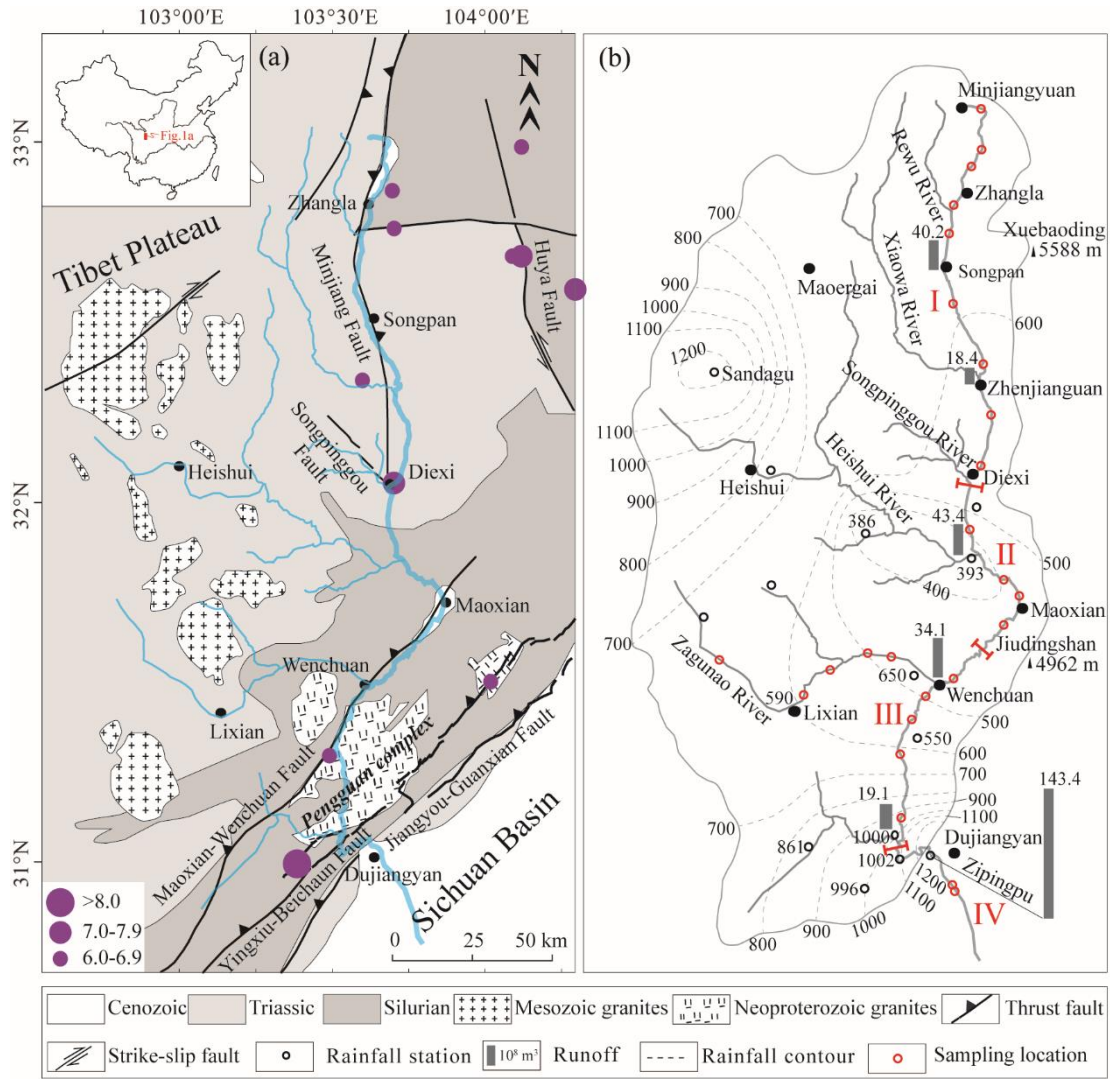
118 2.1 Geographic and geologic settings

119 Instrumental data collected after 1900 indicate that the TP has experienced strong
120 earthquakes clustered around the Bayan Kala Block from 1995 to the present day, which
121 are collectively known as the Kunlun–Wenchuan earthquake series (Deng et al., 2014).

122 The eastern TP is geomorphologically characterized by alpine valleys, and is
123 ~~tectonic~~ally activity is controlled by the Longmen Shan thrust belts, the Minjiang Fault,
124 and the Huya Fault (Fig. 1a). Frequent tectonic activities have led to numerous
125 earthquakes and landslides in this region (e.g., Zhang et al., 2003; Jiang et al., 2014; Li
126 et al., 2015; Liang and Jiang, 2017), such as the 1933 Diexi M_s 7.5 earthquake, the 1976
127 Songpan M_s 7.2 earthquake, the 2008 Wenchuan M_s 8.0 earthquake and the 2017
128 Jiuzhaigou M_s 7.0 earthquake. These earthquakes caused widespread damage ~~at to~~ the
129 Earth surface in this region. GPS–measured uplift rates in the Longmen Shan Fault zone
130 reached 2–3 mm/a over 10 years since 1999 (Liang et al., 2013). Thermochronological
131 dating of zircon and apatite indicated denudation rates of 1–2 mm/a in the Longmen
132 Shan region during the Late Cenozoic (Kirby et al., 2002).

133 The alpine valleys in the eastern TP reduce the preservation potential of
134 Quaternary sediments and expose large areas of bedrock. Bedrock outcrops within the
135 catchment region of the upper Min River are dominated by Silurian phyllite, quartz
136 schist, and Triassic phyllite, metamorphosed sandstone (Fig. 1a), which are easily
137 weathered and eroded into transportable debris (Zhong et al., 2019). Massive granites
138 are also exposed in the study area; in particular, the Neoproterozoic Pengguan complex
139 (U–Pb age of 859–699 Ma; Ma et al., 1996) (Fig. 1a) is mainly composed of
140 intermediate–acid intrusive rocks, with lesser amounts of basic–ultrabasic intrusive

141 rocks, volcanic rocks, volcanoclastic rocks, and greenschist facies metamorphic rocks.
 142 Sand ($> 63 \mu\text{m}$) in the study area was recently demonstrated to have been mainly
 143 derived from local debris material, which itself is likely related to dust storms and loose
 144 surface material produced by seismic activity (Jiang et al., 2017; Liang and Jiang, 2017).



145 **Figure 1** (a) Geological map and (b) precipitation distribution (Ding et al., 2014) for
 146 the upper Min River basin. Seismic data are from the China Earthquake Data Center
 147 (<http://data.earthquake.cn/data>).
 148
 149

150

151 The upstream channel of the Min River is ~340 km long (Li et al., 2005; Ding et

152 al., 2014), nearly oriented N–S (Fig. 1b), and erodes the hinterland of the TP via
153 formation of gullies and valleys. The Min River valley is typically steep, narrow and
154 deepening downstream with an incision depth of 300–1500 m (e.g., Li et al., 2005;
155 Zhang et al., 2005). The slopes on both sides of the study area are between 18° and 45°,
156 and the vertical aspect ratio of the valley is 5.5–12.6 ‰ (Zhang et al., 2005).
157 Constrained by the specific landforms of the alpine valleys, the wind direction in the
158 study area is generally SSW/NNE, roughly consistent with the strike of local valleys
159 (Liu, 2014). The Min River valley exhibits high wind speeds in April (average 4.9 m/s)
160 and low speeds in July (average 3.7 m/s). Wind speed is generally < 4 m/s before noon
161 and > 4 m/s after noon, and normally peaks approximately 8–10 m/s at around 16:00
162 (Liu, 2014). The highest instantaneous wind speed recorded in the study area was 21
163 m/s (Liu, 2014).

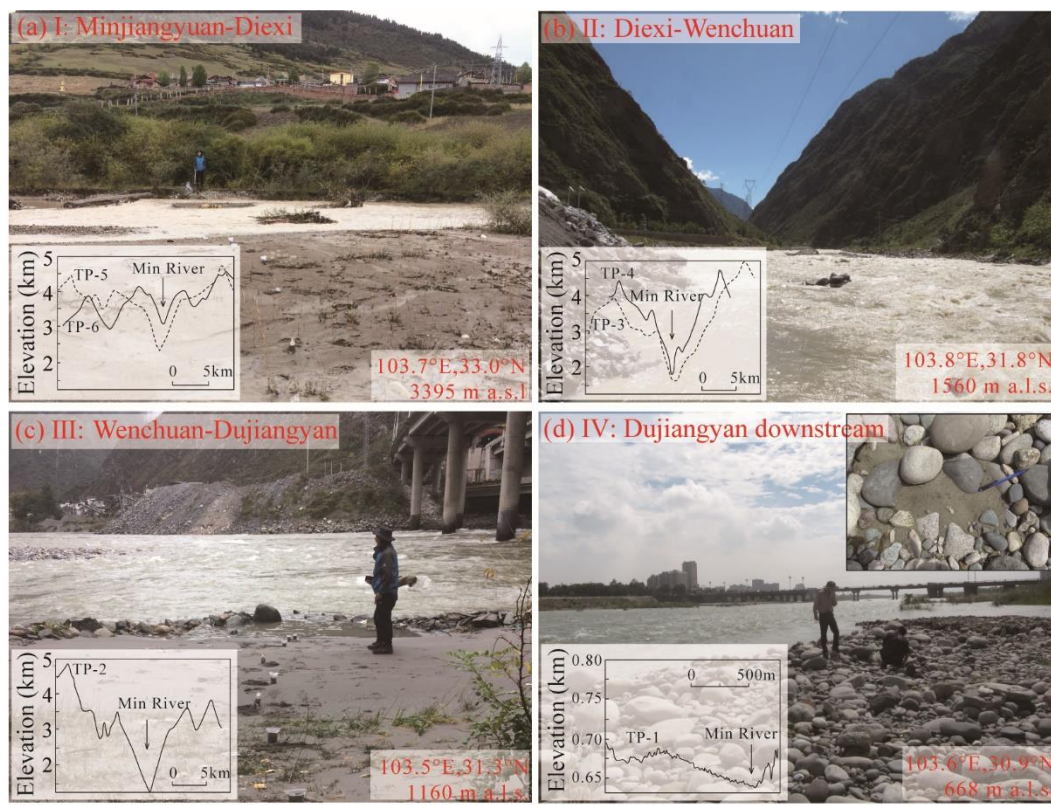
164 The upper reaches of the Min River are located in a transition zone on the TP
165 where wet monsoonal climate changes to a high–elevation cold [regionclimate](#). In this
166 region, mean annual precipitation (MAP) ranges from 400 mm to 850 mm, and
167 precipitation is dominant (>75%) during the rainy season (May–October) (Ding et al.,
168 2014). It is noticeable that orographic rain along the eastern TP generates two storm
169 areas centered around Sandagu and Zipingpu (Fig. 1b). Statistical analyses of
170 precipitation data from 1982 to 2007 show that the MAP within these regions is higher
171 than 1200 mm (Ding et al., 2014).

172 Regional vegetation has clear vertical zonation, which mainly consists of small–
173 leaf, arid shrubs at 1300–2200 m a.s.l., mixed broadleaf–conifer forests, evergreen and
174 deciduous broad–leaved mixed forests at 2000–2800 m a.s.l., *Picea* and *Abies* forests
175 at 2800–3600 m a.s.l., and alpine shrubs and meadows at > 3600 m a.s.l. (Ma et al.,
176 2004; Zhang et al., 2008; [Wei et al., 2021](#); [Xu et al., 2020](#)). There are two key factors

177 that influence vegetation distribution and ecological conditions in the study area: the
 178 arid and windy climate, which has a large temperature difference between day and night,
 179 and tectonics activity characterized by frequent earthquakes (Lin, 2008; Wang et al.,
 180 2011). For example, strong earthquakes often induce landslides that can destroy
 181 vegetation cover in the study area (Xu et al., 2012, 2014). Both of these factors lead to
 182 fragility in landscape and vegetation cover.

183 2.2 Segmented characteristics of the Min River

184 Based on the topographical and geomorphological characteristics, ~~and~~ fault and
 185 vegetation distribution patterns, ~~of~~ the upper Min River ~~allow it to~~ could be subdivided
 186 into four segments: I, II, III, and IV (Fig. 1b).



187
 188 **Figure 2** Photographs of field sampling sites in the upper Min River. The locations of
 189 cross-sections through the Min River valleys (Zhang et al., 2005) are shown in Fig. 7c.

190

191 Segment I is the Minjiangyuan – Diexi segment (3460–2190 m a.s.l.). The riverbed

192 in this segment is directly connected with one side of the Min Mountain and has a valley
193 bottom width of 200–1000 m (Zhang et al., 2005) (Fig. 2a). Downstream from ~~the~~
194 Minjiangyuan, valley bottom width narrows markedly and is only 200–300 m in
195 Zhenjiangguan – Diexi segment (Zhang et al., 2005). The relative relief of the Min
196 Mountain increases significantly from Minjiangyuan to Diexi along the Min River,
197 especially from ~~the~~ Zhenjiangguan to Diexi (Zhang et al., 2005). The vegetation
198 coverage along this segment gradually deteriorates, with *Picea*, *Abies*, shrubs, and herbs
199 in the Minjiangyuan – Songpan segment, but only a small number of shrubs and herbs
200 in the Songpan – Diexi segment. Bedrock is widely exposed in the lower part of the
201 segment. In this region, the monthly maximum wind speed reaches 15.4 m/s in Songpan.

202 Segment II is the Diexi – Wenchuan segment (2190–1470 m a.s.l.). The valley
203 bottom width in this segment ~~continuously~~ decreases to 200–300 m (Zhang et al., 2005),
204 and the Min Mountains always occur in direct contact with the riverbed of the Min
205 River (Fig. 2b). The longitudinal slope (12.6‰) reaches its maximum regional value
206 near Diexi (Zhang et al., 2005). The regional vegetation coverage is mostly sparse and
207 the bedrock is ~~naked~~ well exposed.

208 Segment III is the Wenchuan – Dujiangyan segment (1470–900m a.s.l.). The valley
209 bottom width in this segment widens to about 200–500 m (Zhang et al., 2005) (Fig. 2c)
210 and regional vegetation cover increases compared to segment II. In particular, the
211 hillside around the Zipingpu Reservoir is covered with thick broad-leaved trees and
212 herbs. The monthly maximum wind speed in Lixian is 14.0 m/s.

213 Segment IV is the Dujiangyan – segment (900 – 630 m a.s.l.). This segment flows
214 into the interior of the Sichuan Basin, where it has flat geomorphological features (i.e.,
215 the riverbed width is greater than 300 m; Fig. 2d), and then transitions into the middle
216 reach of the Min River. The monthly maximum wind speed in Dujiangyan is 13.8 m/s.

217

218 **3 Materials and methods**

219 **3.1 Field sampling and grain-size analysis**

220 A ~~~265~~340 km transect along the upper Min River was conducted during October
221 2017, starting in the eastern TP (Minjiangyuan, 33°01'59"N, 103°42'42"E; 3462 m a.s.l.)
222 and ending in the Sichuan Basin (Dujiangyan, 30°56'25"N, 103°38'14"E; 634 m a.s.l.)
223 (Fig. 1b). A total of 181 river samples were collected for grain-size analysis at 25 sites
224 (Table S1). Sampling sites were selected from exposed, freshly-developed depositional
225 sequences that occurred close to the active channel and its margins (Fig. 2). Voluminous
226 bedrock gravel occurs around the sampling sites (Fig. 2). To ensure sample consistency
227 associated with uniform flow regimes, each sample was collected at a depth of 0–0.2 m
228 from different places within each sampling sequence. All locations were carefully
229 chosen to avoid contamination from riverbank materials or from anthropogenic
230 reworking.

231 Grain-size analysis was conducted using a Malvern Master-sizer 3000 laser
232 grain-size analyzer at the State Key Laboratory of Earthquake Dynamics, Institute of
233 Geology, China Earthquake Administration in Beijing, China. About 0.5 g of sediment
234 was pretreated with 20 ml of 30% H₂O₂ to remove organic matter and then with 10 ml
235 of 10% HCl to remove carbonates. About 300 ml of deionized water was added, and
236 the sample solution was kept for 24 h to rinse acidic ions. The sample residue was
237 dispersed with 10 ml of 0.05 M (NaPO₃)₆ on an ultrasonic vibrator for 10 min before
238 grain-size measurements. For each sample, the grain-size analyzer automatically

239 outputs the median diameter (Md) and the percentages of each size fraction, with a
240 relative error of less than 1%. Magnetic susceptibility (SUS) was measured using a
241 Bartington MS2 susceptibility meter.

242 **3.2 Y values**

243 Mean grain size (Ms), standard deviation (σ), skewness (Sk), and kurtosis (K_G) are
244 commonly used to discriminate between different depositional processes and
245 environments. Sahu (1964) distinguished aeolian processes from those that operate in a
246 littoral environment by using the following equation:

$$247 \quad Y = -3.5688 Ms + 3.7016 \sigma^2 - 2.0766 Sk + 3.1135 K_G \quad (1)$$

248 Here, Y values less than -2.74 indicate an aeolian provenance and Y values greater
249 than -2.74 indicate a hydrogenic provenance (Sahu, 1964). Calculated Y values for
250 lacustrine sediments (Jiang et al., 2017, 2014), red clay, and loess–paleosol deposits
251 (Wu et al., 2017; Lu and An, 1999) are less than -2.74 , indicating an aeolian provenance.

252 **3.3 End–member analysis**

253 Numerical unmixing of grain–size distribution data into constituent components,
254 known as end–member analysis (EMA), can yield valuable information about transport
255 dynamics (Weltje, 1997; Paterson and Heslop, 2015; Jiang et al., 2017). According to
256 the principle that the end–member number (EM) should be as small as possible (Weltje
257 et al., 1997), several EMs obtained by end–element analysis imply that numerous
258 dynamic mechanisms occurred during formation of these deposits. Generally, larger
259 values of EMs correspond to a stronger transport capacity, which itself indicates
260 different provenances (Vandenberghe, 2013; Dietze et al., 2014; Jiang et al., 2017). For
261 instance, the peak values of EMs in Lixian lacustrine sediments were concentrated at

262 10 μm (EM_1) and 40 μm (EM_2), and so reflect the background deposition of dust and
263 locally sourced deposition transported by ambient wind, respectively (Jiang et al., 2017).
264 We analyzed the Min River samples using the AnalySize software for processing and
265 unmixing grain-size data (Paterson et al., 2015), with parameters selected from the
266 generalized Gaussian skewness model (SGG) (Egli, 2003).

267 **3.4 Analysis of C–M and F–M diagrams**

268 The analysis of C–M and F–M diagrams is useful to interpret sediment transport
269 dynamics (Passega, 1957; Singh et al., 2007). In these diagrams, C is the coarsest
270 percentile of the grain-size distribution in samples (one percentile), and M is the median
271 diameter of the grain-size distribution, which are both indicators of the maximum and
272 average transport capacity, respectively (Passega, 1957; Singh et al., 2007; Bravard et
273 al., 2014). In addition, F represents the percentage of fractions finer than 125 μm (Singh
274 et al., 2007). All values are plotted on a logarithmic scale, which produces specific
275 patterns for distinct reaches (Singh et al., 2007; Bravard et al., 2014). A C–M diagram
276 (Fig. S1) has the following sections: NO, rolling; OP, rolling with some grains
277 transported in suspension; PQ, graded suspension with some grains transported by
278 rolling; QR, graded suspension; RS, uniform suspension; and T, pelagic suspension
279 (Passega, 1957; Bravard and Peiry, 1999; Bravard et al., 2014).

280

281 **4 Results**

282 **4.1 Characteristics of grain-size and SUS**

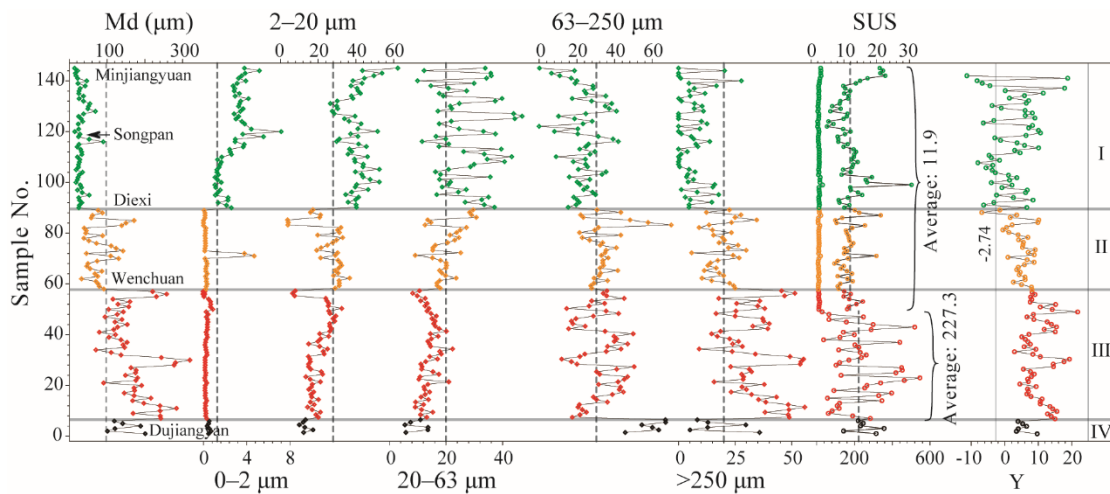
283 The median grain size (M_d), five grain-size fractions (0–2 μm , 2–20 μm , 20–63 μm ,

284 63-250 μm , >250 μm), SUS and Y values of the Min River sediment can be divided
 285 into four categories (Fig. 3), which correspond to the different segments (I–IV) defined
 286 above. The average values of Md increased significantly at Diexi (from 31.0 μm to 80.8
 287 μm) and Wenchuan (from 49.3 μm to 170.2 μm), and decreased slightly at Dujiangyan
 288 (from 220.4 μm to 119.2 μm). The variations at these three sites are the most significant
 289 within the whole river (Table 1, Fig. 3).

Table 1 Statistics for grain-size fractions in the upper Min River.

Segments	Md (μm)	Percentage composition / (%)					SUS
		0–2	2–20	20–63	63–250	>250	
		μm	μm	μm	μm	μm	
I	31.0	2.8	40.3	27.1	23.7	6.2	11.6
II	80.8	0.4	25.3	20.3	34.6	19.4	11.3
III	170.2	0.3	20.0	13.9	31.9	33.8	193.5
IV	145.2	0.5	13.0	9.5	59.5	17.5	251.8

291
292



293 **Figure 3** Variation of grain-size components and river sediment parameters from the
 294 upper Min River. The dotted lines represent the average value of the whole sequence.

295

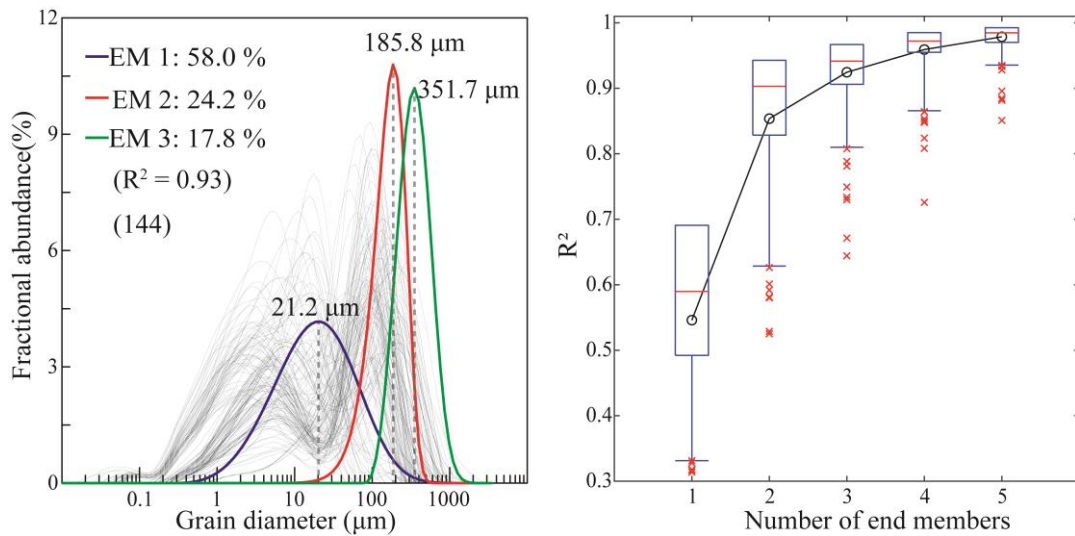
296 Along the upper Min River downwards, the mean proportion of the 2–20 μm (I =

297 40.3%, II = 25.3%, III = 20.0%, and IV = 13.0%) and 20–63 μm fractions (I = 27.1%,
298 II = 20.3%, III = 13.9%, and IV = 9.5%) exhibit a stepwise decrease (Table 1, Fig. 3).
299 The 63–250 μm fraction exhibits a sharp increase from segment I (23.7%) to II (34.6%)
300 and from segment III (31.9%) to IV (59.5%), but a relatively minor change from
301 segment II (34.6%) to III (31.9%) (Table 1, Fig. 3). The > 250 μm fractions exhibit a
302 stepwise increase between segments I, II, and III (6.2%, 19.4%, and 33.8%,
303 respectively), and a significant decrease from segment III (33.8%) to IV (17.5%) (Table
304 1, Fig. 3). Measured SUS values remained low in segments I (5.3–30.6, with a mean of
305 11.6) and II (7.1 to 21.2, with a mean of 11.3), but were significantly higher in segment
306 III (9.9–546.5, with a mean of 193.5) and reached consistently high values in segment
307 IV (142.1–356.5, mean: 251.8) (Table 1, Fig. 3).

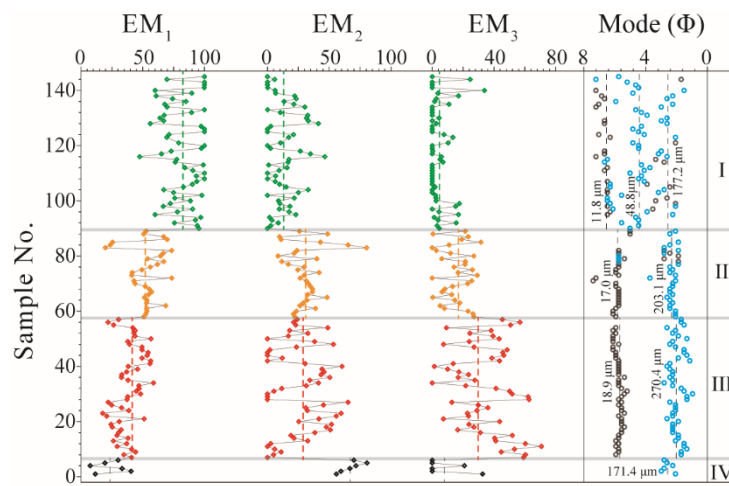
308 4.2 End–member analysis

309 Three end–members (EMs) ($R^2 = 0.93$) were identified in the Min River samples
310 (Fig. 4) with peaks of 21.2 μm (58.0%), 185.8 μm (24.2%), and 351.7 μm (17.8%),
311 respectively. Along the upper Min River downwards, these three EMs show clear
312 stepwise changes between segments (Fig. 5). EM₁ shows a stepwise decrease (I = 82.5%,
313 II = 53.1%, III = 38.6%, and IV = 23.7%), corresponding to the sum of the 2–20 μm
314 and 20–63 μm fractions (Figs. 3, 5). EM₂ shows a sharp increase from segment I (13.1%)
315 to II (31.4%) and from segment III (27.1%) to IV (67.4%), and a relatively smaller
316 change from segment II (31.4%) to III (27.1%), corresponding to the 63–250 μm
317 fraction. By contrast, EM₃ corresponds to the >250 μm fraction (Figs. 3, 5) and shows
318 a stepwise increase between segments I, II, and III (4.4%, 15.5% and 38.6%,

319 respectively), and a significant decrease from segment III (38.6) to IV (23.7%).



320 **Figure 4** End-member analysis model of fluvial sediments from the upper Min River.



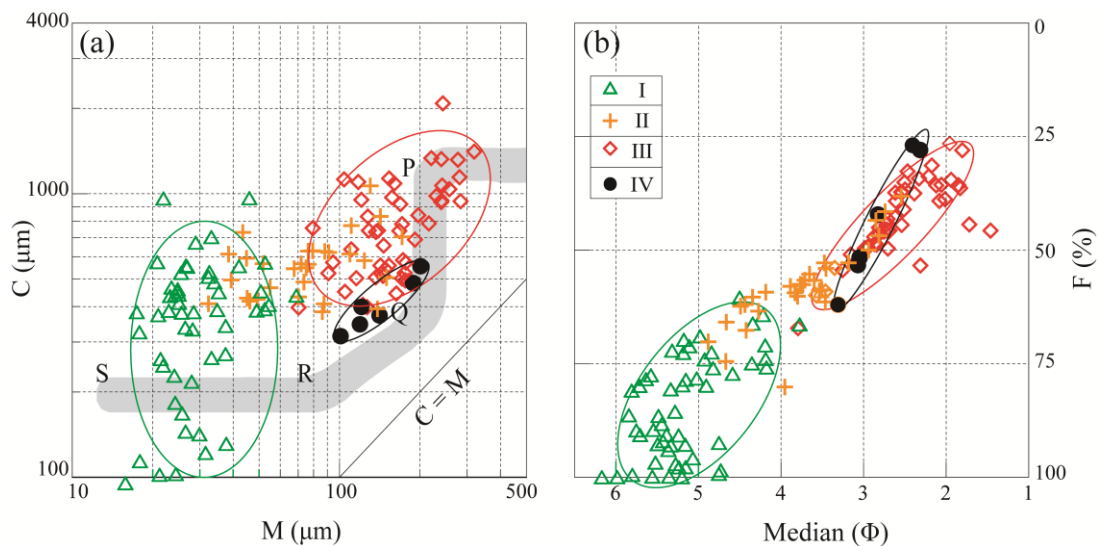
321
 322 **Figure 5** Variability of ~~three~~ EMs and ~~their~~ mode values of samples collected from the
 323 upper Min River. ~~The fractional abundance (>1%) of the peak~~ The peak values (mode
 324 values) with >1% fractional abundance of ~~in~~ the grain-size frequency distributions were
 325 extracted after consideration of a 1% instrumental error. ~~Blue~~ Black and gray circles
 326 represent the main and secondary peak modal values, respectively. The dotted lines
 327 represent the average value.

328

329 4.3 Characteristics of the grain-size frequency distribution

330 The grain-size frequency of river samples from segment I has a discrete

331 distribution (Fig. S2) with three mode values at $\sim 11.8 \mu\text{m}$, $\sim 48.8 \mu\text{m}$, and $\sim 177.2 \mu\text{m}$.
 332 The main mode value of segment I occurred in the $\sim 48.8 \mu\text{m}$ portion. The grain-size
 333 frequency distribution for segments II and III is strongly bimodal (Fig. S2), with the
 334 major and minor mode values at $\sim 203.1 \mu\text{m}$ and $\sim 17.0 \mu\text{m}$ for segment II, and ~ 270.4
 335 μm and $\sim 18.9 \mu\text{m}$ for segment III. The grain-size frequency distribution for segment
 336 IV is unimodal (Fig. S2) with a mode value of $\sim 171.4 \mu\text{m}$.
 337



338 **Figure 6** C–M and F–M distributions of samples collected from ~~the four studied~~
 339 ~~segments of~~ the upper Min River.

340

341 4.4 C–M and F–M diagrams

342 On a C–M diagram for the Min River, samples from segment I are completely
 343 separate from those collected from segments III and IV. Most samples in segment II
 344 overlap with those of segment III (Fig. 6a). Among them, the M value of segment I
 345 ($13.9\text{--}89.8 \mu\text{m}$) mainly belongs to the RS section (Fig. 6a), although the C values
 346 exhibit a large variation between $54.8 \mu\text{m}$ and $964.3 \mu\text{m}$. Samples from segment II are

347 distributed throughout the P–Q–R sections (Fig. 6a), have C values of 383.5–1066.0
348 μm , and M values of 32.2–171.4 μm . Samples from segment III are concentrated in the
349 PQ section (Fig. 6a), have C values of 396.9–2083.8 μm , and M values of 70.3–319.1
350 μm . Samples in segment IV plot close to the RQ section and are distributed parallel to
351 the $C = M$ line (Fig. 6a). Samples collected from segments of the Min River show
352 similar distribution features in F–M diagrams to those shown in C–M diagrams (Fig.
353 6).

354

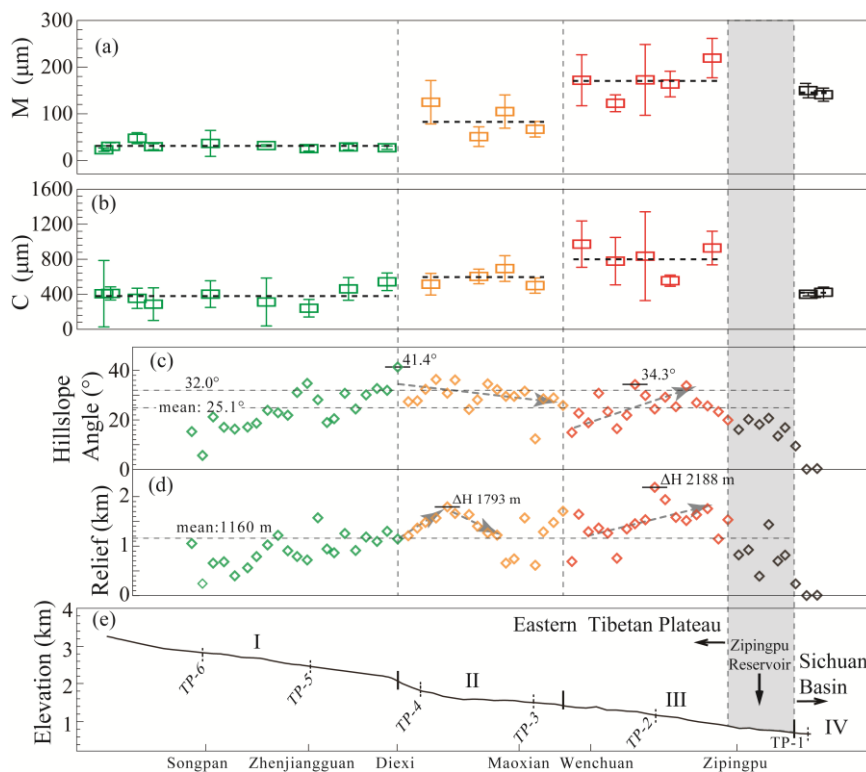
355 **5 Discussion**

356 **5.1 Dynamic and provenance implications of fluvial sediments**

357 Grain–size fractions, EMs, and mode values in different segments along the upper
358 reaches of Min River reflect the distinct provenance and transport dynamics of fluvial
359 sediments (McKinney and Sanders, 1978; Sun et al., 2002, 2004; Sun et al., 2007;
360 Dietze et al., 2014; Vandenberghe, 2013). The EM_1 in segment I reaches a proportion
361 of 82.5%, which corresponds to the fine particle components ($<63 \mu\text{m}$ fractions).
362 Previous studies have indicated that fractions with sizes of $<10 \mu\text{m}$ and $10\text{--}40 \mu\text{m}$
363 represent background particles and regional dust that have been transported by wind
364 (Dietze et al., 2014; Jiang et al., 2014, 2017), which contribute $51\pm 11\%$ and $42\pm 14\%$
365 of the lacustrine sediments across the TP, respectively (Dietze et al., 2014). Therefore,
366 the EM_1 (fine–grained fractions) in segment I probably have an aeolian provenance.
367 This inference is supported by five separate lines of evidence: 1) Md varies within the
368 narrow range $13.9\text{--}89.8 \mu\text{m}$ (Fig. 3), although the C values fluctuate widely between

369 54.8 μm and 964.3 μm (Fig. 7); 2) the distribution of samples in an RS section in a C–
 370 M diagram (Fig. 6) reflects uniform suspension, which likely requires transportation by
 371 ubiquitous and strong wind (Fig. S1, Passega, 1957); 3) nearly half of the samples (i.e.,
 372 22 out of 55) have Y values of less than -2.74 , which is indicative of an aeolian origin
 373 (Sahu, 1964); 4) loess deposits are widely distributed in the study area, especially from
 374 Diexi upstream (Fig. S3) (Liu et al., 2013; Shen et al., 2017) and may represent a
 375 voluminous source of dust particles; and 5) the study area has a high mean altitude of
 376 2840 m, and the monthly maximum wind speed can reach 15.4 m/s, which would allow
 377 for strong aeolian transport.

378



379 **Figure 7** Variation characteristics of **(a)** M and **(b)** C values of the grain-size index. **(c)**
 380 Riverbed base-level and the position of the cross-section of the upper Min River
 381 (Zhang et al., 2005). **(d)** Hillslope angle and **(e)** local relief along the upper Min River.

382 A 4*4 km grid was delineated along the upper Min River (~260 km). The highest
383 ridgeline and riverbed height in the grid were extracted from a DEM map, and the local
384 relief was then obtained by calculating the highest ridgeline minus the riverbed height.
385 The hillslope angle was obtained by solving for \tan (local relief/slope length).

386 The EM₂ in segment IV reaches the highest value (185.8 μm : 67.4%) recorded in
387 the whole sequence and corresponds to the 63–250 μm fraction (59.5%), which is
388 consistent with previous studies having shown that fluvial deposits are composed
389 mainly of a medium–sand component (modal size: 200–400 μm) (Middleton, 1976;
390 Tsoar and Pye, 1987; Bennett and Best, 1995; Dietze et al., 2014). In the C–M diagram,
391 sample data that lie close to the C = M line reflect the suspension transport of riverbed
392 sediments (Fig. 6a) (Singh et al., 2007; Passega, 1957). In addition, the single peak
393 mode (Fig. S2d) of segment IV represents a single river transport process and
394 sedimentary environment (McKinney and Sanders, 1978), and the small size range of
395 the grain–size frequency distribution also reflects a well–sorted product that was
396 deposited by fluvial action (Sun et al., 2002). Therefore, the EM₂ mainly reflect typical
397 fluvial sediments.

398 EM₃ corresponds to the coarsest grain–size components (>250 μm) and has the
399 highest value (351.7 μm : 38.6%) of the whole sequence in segment III. The maximum
400 values of C and M (Figs. 7a, b) in segment III indicate that it had the highest transport
401 capacity (Passega, 1957; Singh et al., 2007; Bravard et al., 2014). Therefore, EM₃
402 represents the local sedimentary component that was locally transported over short
403 distances (Dietze et al., 2014; Jiang et al., 2014, 2017). The distribution characteristics

404 of samples from segment III in the PQ section (Fig. 6a) indicate that dominant rolling
405 and jumping transportation processes ~~dominated~~ (Passega, 1957). Meanwhile, the SUS
406 values in segment III increase to abnormally high values (28.5–546.5, with a mean of
407 227.3) abruptly near to exposures of the Pengguan complex (Fig. 1a), although lower
408 SUS values occur in the surrounding area (Zagunao River: 9.1–114.1, with a mean of
409 34.1, Fig. S4; Zipingpu reservoir: 5–60, Zhang et al., 2019; and segments I and II: 5.3–
410 30.6, mean 11.5, Fig. 3). The precipitation in segment III is generally low (400–700
411 mm/a) and only significantly increases near to the Zipingpu reservoir (1200 mm/a), so
412 that the sedimentary changes were muted until 2 years after the Wenchuan earthquake
413 (Zhang et al., 2019) (Fig. 1b). In addition, the mean grain size in segment III (170.2 μm)
414 increases before the Zagunao River (mean of 83.1 μm , Fig. S4) joins the Min River (Fig.
415 1b. 3) and contribution from the Zagunao River can be precluded. Therefore, the
416 abnormally high grain size and SUS values in segment III are likely caused by a local
417 provenance change.

418 **5.2 Climate controlled fine-grained fluvial sediments**

419 The windy and semi-arid climate in the study area is responsible for more fine
420 particle components (EM_1) in segment I (Jiang et al., 2014), which caused EM_1 to
421 gradually decrease downstream as the wind weakens (Fig. 5). The relatively low
422 precipitation (400–700 mm/a) and low runoff ($18.4\text{--}43.4 \times 10^8 \text{ m}^3$) (Fig. 1b) in segment
423 I reflect the limited transport capacity of the river, and the angular gravels on the
424 riverbed also indicate weak scouring, which preserves more fine-grained components
425 (EM_1) in fluvial sediments. Segment I developed along the Minjiang Fault (Fig. 1a),

426 which has a low slip rate (0.30–0.53 mm/a, Kirby et al., 2000; Zhou et al., 2000, 2006;
427 Tan et al., 2019) and therefore a weak influence on local provenance supply (Jiang et
428 al., 2014, 2017). In addition, the wide riverbed (Fig. 2a), relatively low hillslope angle,
429 and local relief in the Minjiangyuan–Songpan segment (Figs. 7d, e) causes *in situ*
430 retention of locally sourced coarse components. Therefore, EM₂ and EM₃ make only a
431 minor contribution to the fluvial sediments in segment I.

432 Segment IV is located inside the Sichuan Basin and is completely unaffected by
433 alpine valleys in the eastern TP. It is characterized by a wide and flat geomorphological
434 surface (Fig. 2d). The significant downstream increase in precipitation and runoff in the
435 Zipingpu reservoir (Fig. 1b) indicates that fluvial action was the main control on
436 sediment transportation in segment IV. **In addition, well-rounded pebbles (Fig. 2d) on**
437 **the riverbed prove this point.**

438 **5.3 Coarse-grained deposits controlled by tectonism**

439 Fluvial sediments coarsen at the transition between segments I and II, highlighting
440 an increase in EM₂ and EM₃ content, and a higher M value (Figs. 3, 7). This locality
441 occurs at intersection of the Minjiang Fault and the Songpinggou Fault (Fig. 1a), which
442 was the epicenter of the Diexi *M_s* 7.5 earthquake in 1933 (Chen et al., 1994; Ren et al.,
443 2018). As a result, the outcropping bedrock was severely damaged and so provided new,
444 fresh, and local sediment sources (EM₃). Downstream from Diexi, field surveys exhibit
445 that the altitude decreases by 400 m over a horizontal distance of 20 km, such that the
446 longitudinal slope of the riverbed (12.6‰, Fig. 7c, Zhang et al., 2005) and the hillslope
447 angle (41.4°, Fig. 7d) are highest in this region when compared to the entire study area,
448 which imply a higher ~~of rivers incision rates~~ regional denudation rate forced by active
449 tectonics (Zhang et al., 2005; Whittaker et al., 2007a). These remarkable changes of

450 geomorphology correspond well to a twofold increase in erosion coefficients that occur
451 within 15 km of major faults in the eastern TP (Kirkpatrick et al., 2020) and more
452 intense denudation at the location of seismogenic faulting along high-relief plateau
453 margins (Li et al., 2017). The narrower valley and direct contact between the riverbed
454 and hillside on either side in segment II (Fig. 2b) provide favorable conditions for
455 rolling and jumping transportation of sediment along the hillslope. In addition, the rapid
456 rising of the base-level of the Min River in segment II enhances the river's cutting and
457 transport capacity (Merritts and Vincent, 1989; Stokes et al., 2002; Cheng et al., 2004;
458 Whittaker et al., 2007a; Boulton et al., 2014).

459 ~~Measured~~ EM₃ rapidly reaches its maximum fluctuation range in segment III (Fig.
460 5), likely due to the maximum transport force (C value) in the area (Fig. 7). The regional
461 precipitation in segment III is low (400–700 mm/a) and only significantly increases
462 near to the Zipingpu reservoir (1200 mm/a) (Fig. 1b). From a tectonic perspective, the
463 Maoxian–Wenchuan Fault, with a large dextral slip rate (1.0–3.8mm /a; Chen and Li,
464 2013; Wang et al., 2017) and a large vertical slip rate (~1–2 mm/a; Liu et al., 2015),
465 mainly controls the distribution of segment III (Fig.1). Previous studies have shown that
466 the Maoxian–Wenchuan Fault occurs a band of maximum exhumation along the
467 eastern Longmen Shan Fault zone since the late Miocene (Tan et al., 2019). Therefore,
468 rapid regional uplift and denudation (Kirby et al., 2002; Liang et al., 2013) not only
469 generated a larger hillslope angle (mean value of 24.9°) and the highest local relief
470 (2188 m), but also provided widespread source of fresh, coarse-grained, and local
471 sediment (Whittaker et al., 2007b, 2010) in segment III. The significant coarsening of
472 fluvial sediment at the beginning of segment III indicates the catchments undergoing a

473 transient response to tectonics are associated with significant volumetric export of
474 material (Whittaker et al., 2010). Moreover, the PQ distribution of segment III samples
475 in the calculated C–M diagram (Fig. 4) shows the importance of rolling and jumping
476 transport mechanisms (Passega, 1957), which correlate with the steep landform features
477 in segment III (Fig. 2c). Exposures of hard Mesozoic granites instantaneously provide
478 a local source of coarse components, and thus correspond to the maximum M and C
479 values. Although regional climate generally has a weak influence on the supply of
480 coarse particles, the concentrated distribution of particles within the calculated grain–
481 size frequency distribution (Fig. S2c) indicates that fluvial action played an effective
482 role in sorting local sediment sources (Sahu, 1964; Sun et al., 2002; Frings, 2008). The
483 persistent occurrence of the coarsest grain–size cross the segment III responds to the
484 fact that the catchments crossing faults maintain their high slip rate over time, which
485 exhibits a sharp contrast to that of segment I.

486 Generally, a large earthquake is followed by a period of enhanced mass wasting
487 and fluvial sediment evacuation (Hovius et al., 2011; Wang et al., 2015). The Wenchuan
488 *M*_s 8.0 earthquake in 2008 caused severe geomorphological damage in region, and the
489 annual average suspended sediment flow in regional rivers increased by a factor of 3–
490 7 following the earthquake. The river recovered to its pre–earthquake level just $1.2 \pm$
491 0.9 years later (Wang et al., 2015), ~~).~~ ~~however~~ However, over 70% of the co–seismic
492 debris has stabilized in place along the hillslopes during the following decades (Dai et
493 al., 2021) and will take 370 years to be removed out of the mountains (Wang et al.,
494 2017). As such, we believe that co–seismic debris generated by the Wenchuan

495 earthquake in 2008 had negligible influence on our sample collection campaign
496 conducted in 2017.

497 **5.4 Geomorphic morphology reveals tectonic activity**

498 Alpine valleys characterize the landscape of the upper reaches of the Min River in
499 the eastern TP (Figs. 2, 7) and have an incision depth of 300–1500 m (Li et al., 2005;
500 Zhang et al., 2005) (Fig. 6a). In segment I, hillslope angles and local relief gradually
501 increase downstream along the Minjiang Fault from 5° to 34.8° and 243 m to 1572 m,
502 respectively (Figs. 7d, e). However, these changes seem ~~a little contradict with the~~
503 ~~consistent high to be decoupled with the high and stable~~ proportion of fine-grained
504 background dust in the fluvial sediments of segment I (Figs. 3, 5), which is an open and
505 interesting question. The consistent precipitation and runoff rates explain the calculated
506 consistency in transport power, as defined by unchanging values of C and M (Fig. 7).
507 We note that the longitudinal slope of the riverbed (6.7–7.6‰, Fig. 7c; Zhang et al.,
508 2005) in segment I steadily changes as altitude decreases from 3460 m to 2190 m;
509 therefore, gradual steepening of the landscape is likely a response to enhanced river-
510 related erosion (Merritts and Vincent, 1989; Stokes et al., 2002; Cheng et al., 2004).
511 The high vegetation density in the Minjiangyuan – Songpan region is also probably
512 modulated by the lower topographic slope (Figs. 2a, 7) (Olen et al., 2016). These are
513 consistent with generally weak activity of the Minjiang Fault (Kirby et al., 2000; Zhou
514 et al., 2000, 2006; Tan et al., 2019).

515 In segment II, the hillslope angle (12.3–41.4°, with a mean of 30.1°) is generally
516 steeper than the average for the whole study area (25.1°), and the highest angles (41.4°)

517 far exceed the stability threshold of $\sim 32^\circ$ for landslide denudation, which suggests that
518 landslide-dominated hillslope denudation has kept pace with the rates of rock uplift and
519 valley incision in segment II (Burbank, et al., 1996; Montgomery and Brandon, 2002;
520 Clarke and Burbank, 2010; Wang et al., 2014). Along the studied transect, local relief
521 in segment II initially increases and then decreases (Fig. 7c), and the flow direction of
522 the Min River also changes from roughly N–S to NW–SE (Fig. 1a). The lithology in
523 segment II changes from Triassic to Silurian (Fig. 1a), and seismic activity transitions
524 from the Minjiang Fault to the Maoxian–Wenchuan Fault. Given that segment II records
525 the lowest annual rainfall in the study area (< 500 mm/a, Fig. 1), this transformation of
526 tectonic activity and lithology likely plays a dominant role on fluvial erodibility (Selby,
527 1980; Stokes et al., 2008; Whittaker et al., 2007a; Zondervan et al., 2020), and
528 influences changes ~~in~~of regional geomorphology and river drainage.

529 Hillslope angles (14.9° – 34.3° , with a mean of 24.9°) and local relief (689–2188 m,
530 with a mean of 1463 m) in segment III exhibit a general increase along the Maoxian–
531 Wenchuan Fault (Figs. 1, 7), although they differ from the increasing trends shown in
532 segment I. For example, the highest local relief ~~encountered~~ throughout the entire
533 sequence occurs in segment III, although its mean hillslope angle (24.9°) is lower than
534 the mean value (25.1°) ~~for~~of the entire sequence (Fig. 7). In addition, precipitation and
535 runoff only show a significant increase adjacent to the Zipingpu reservoir (Fig. 1). We
536 note that the regional bedrock in segment III is dominated by hard Mesozoic granites
537 of the Pengguan complex (Fig. 1a), and that the Maoxian–Wenchuan Fault is situated
538 on the zone of maximum exhumation along the Longmen Shan fault zone (Tan et al.,

539 2019). Therefore, the higher local relief along segment III indicates that active
540 Maoxian–Wenchuan Fault (Tan et al., 2019) caused enhanced rock uplift and valley
541 incision (Whittaker et al., 2007a; Tan et al., 2019), which accounts for the largest
542 transport forces (C values, Fig. 7) and the coarsest local components (EM₃, Fig. 5) in
543 this section. Nevertheless, a decrease in the mean hillslope angle within segment III
544 may be attributed to hardening of the exposed bedrock of the Pengguan complex rather
545 than weakening of tectonic activity along the Maoxian–Wenchuan Fault. Even if the
546 shortening rates are generally slow in the eastern TP (Densmore et al., 2008; Zhang,
547 2013) and satellite data may be equivocal, grain-size analysis of fluvial sediments
548 combined with topographic analyses can help guide the identification of regional
549 tectonic activity effectively (Schoenbohm et al., 2004; Kirby et al., 2003, 2008; Tan et
550 al., 2019).

551

552 **6 Conclusion**

553 Grain–size analysis was conducted on modern fluvial sediments of the upper Min
554 River and this information was integrated with vegetation, hydrology, geomorphology
555 (local relief and hillslope) and geology (fault and lithology) data to extract regional
556 climate and tectonic signals in the eastern TP. This procedure identified three segments
557 of tectonic activity along the upper Min River. The Minjiang Fault, situated in the
558 Minjiangyuan–Diexi segment, generally shows weak seismic-tectonic activity. ~~Two~~
559 ~~segments of the~~ The Maoxian-Wenchuan fault-Fault from Diexi to Wenchuan and from
560 Wenchuan to Dujiangyan show enhanced phase of regional tectonic activity, ~~–.~~

561 However, although the segment from Dujiangyan to the Sichuan basin records almost
562 no evidence of tectonic activity.

563 In this study, we report a new approach that can reveal the style of regional tectonic
564 activity by analyzing fluvial sediments collected from tectonically active regions. The
565 novelty of this research method and the reliability of the results in this study provide a
566 key framework with which regional tectonic activity can be revealed through the study
567 of fluvial sediments in other tectonically active localities worldwide.

568

569 **Data availability**

570 Data are available in the figshare database
571 (<https://doi.pangaea.de/10.6084/m9.figshare.17111402>).

572

573 **Author contributions**

574 The paper was written by WS and HCJ with major contributions by HYX. SYM
575 got geomorphic data. WS, HYX and SQZ participated in field surveys and sample
576 collection. SQZ, JWF and XTW conducted laboratory tests and interpreted the results.

577 All authors reviewed and approved the paper.

578

579 **Competing interests**

580 The contact author has declared that neither they nor their co-authors have any
581 competing interests.

582

583 **Acknowledgements**

584 This study was supported by the National Nonprofit Fundamental Research Grant
585 of China, Institute of Geology, China Earthquake Administration (IGCEA2126 and
586 IGCEA1906).

587

588 **References**

589 Beek, V.D., Bishop, P.: Cenozoic river profile development in the upper Lachlan catchment (SE
590 Australia) as a test of quantitative fluvial incision models. *J. Geophys. Res. Solid Earth*,
591 108(B6), 2309, <https://doi.org/10.1029/2002JB002125>, 2003.

592 Bennett, S.J., Best, J.L.: Mean flow and turbulence structure over fixed, two-dimensional dunes:
593 implications for sediment transport and bedform stability. *Sedimentology*, 42(3), 491-513,
594 <https://doi.org/10.1111/j.1365-3091.1995.tb00386.x>, 1995.

595 Blanckenburg, F.: The control mechanisms of erosion and weathering at basin scale from
596 cosmogenic nuclides in river sediment. *Earth Planet. Sci. Lett.*, 237, 462-479,
597 <https://doi.org/10.1016/j.epsl.2005.06.030>~~[10.1016/j.epsl.2005.11.017](https://doi.org/10.1016/j.epsl.2005.11.017)~~, 2005.

598 Boulton, S.J., Stokes, M., Mather, A.E.: Transient fluvial incision as an indicator of active faulting
599 and Plio-Quaternary uplift of the Moroccan High Atlas. *Tectonophysics*, 633(1), 16-33,
600 <https://doi.org/10.1016/j.tecto.2014.06.032>, 2014.

601 Bravard, J.P., Goichot, M., Tronchère, H.: An assessment of sediment-transport processes in the
602 Lower Mekong River based on deposit grain sizes, the CM technique and flow-energy data.
603 *Geomorphology*, 207, 174-189, <https://doi.org/10.1016/j.geomorph.2013.11.004>, 2014.

604 Burbank, D. W., Blythe, A. E., Putkonen, J., Pratt-Sitaula, B., Gabet, E., Oskin, M., Barros, A., Ojha,
605 T. P.: Decoupling of erosion and precipitation in the Himalayas. *Nature*, 426(6967), 652-655,
606 <https://doi.org/doi:10.1038/nature02187>, 2003.

607 Burbank, D.W., Fielding, E., Anderson, R.S., Brozovic, N., Reid, M. D.C., Leland, J.: Bedrock
608 incision, rock uplift and threshold hillslopes in the northwestern Himalayas. *Nature*, 379(6565),
609 505-510, <https://doi.org/10.1038/379505a0>, 1996.

610 Chen, H., Li, Y.: Water system responding to the dextral strike-slipping of the Longmen Shan fault

611 zone in the upper Min River basin. *J. Mount. Sci.*, 31(2), 211-217,
612 <https://doi.org/10.3969/j.issn.1008-2786.2013.02.010>, 2013 (in Chinese).

613 Chen, S.A., Michaelides, K., Grieve, S.W.D., Singer, M.B.: Aridity is expressed in river topography
614 globally. *Nature*, 573, 573-577, <https://doi.org/10.1038/s41586-019-1558-8>, 2019.

615 Chen, S.F., Wilson, C., Deng, Q.D., Zhao, X.L. Zhi, L.L.: Active faulting and block movement
616 associated with large earthquakes in the Min Shan and Longmen Mountains, northeastern
617 Tibetan Plateau. *J. Geophys. Res. Solid Earth*, 99(B12), 24025-24038,
618 <https://doi.org/10.1029/94JB02132>, 1994.

619 Chen, Z., Burchfiel, B.C., Liu, Y., King, R.W., Royden, L.H., Tang, W., Wang, E., Zhao, J., Zhang,
620 X.: Global positioning system measurements from eastern Tibet and their implications for
621 India/Eurasia intercontinental deformation. *J. Geophys. Res. Solid Earth*, 105(B7), 16215-
622 16227, <https://doi.org/10.1029/2000jb900092>, 2000.

623 Cheng, S.P., Deng, Q.D., Li, C.Y., Yang, G.Z.: Dynamical mechanism, physical erosion processes
624 and influence factors of fluvial incision: A review and prospect. *Quat. Sci.*, 24, 421-429,
625 <https://doi.org/10.1007/BF02873097>[10.3321/j.issn:1001-7410.2004.04.008](https://doi.org/10.3321/j.issn:1001-7410.2004.04.008), 2004 (in
626 Chinese), 2004.

627 Clapp, E.M., Bierman, P.R., Caffee, M.: Using ¹⁰Be and ²⁶Al to determine sediment generation rates
628 and identify sediment source areas in an arid region drainage basin. *Geomorphology*, 45, 89-
629 104, [https://doi.org/10.1016/S0169-555X\(01\)00191-X](https://doi.org/10.1016/S0169-555X(01)00191-X), 2002.

630 Clapp, E.M., Bierman, P.R., Schick, A.P., Lekach, J., Enzel, Y., Caffee, M.: Sediment yield exceeds
631 sediment production in arid region drainage basins, *Geology*, 28, 995-998,
632 [https://doi.org/10.1130/0091-7613\(2000\)28<995:SYESPI>2.0.CO;2](https://doi.org/10.1130/0091-7613(2000)28<995:SYESPI>2.0.CO;2), 2000.

633 Clarke, B.A., Burbank, D.W.: Bedrock fracturing, threshold hillslopes, and limits to the magnitude
634 of bedrock landslides. *Earth Planet. Sci. Lett.*, 297(3-4), 577-586,
635 <https://doi.org/10.1016/j.epsl.2010.07.011>, 2010.

636 Dai, F.C., Xu, C., Yao, X., Xu, L., Tu, X.B., Gong, Q.M.: Spatial distribution of landslides triggered
637 by the 2008 Ms 8.0 Wenchuan earthquake, China. *J. Asian Earth Sci.*, 40, 883-895,
638 <https://doi.org/10.1016/j.jseaes.2010.04.010>, 2011.

639 Dai, L.X., Scaringi, G., Fan, X.M., Yunus, A.P., Liu, Z.J., Xu, Q., Huang, R.Q.: Coseismic debris
640 remains in the orogen despite a decade of enhanced landsliding. *Geophys. Res. Lett.*,

641 <https://doi.org/10.1029/2021GL095850>, 2021.

642 Deng, Q.D., Cheng, S.P., Ma, J., Du, P.: Seismic activities and earthquake potential in the Tibetan
643 Plateau. *Chinese J. Geophys.*, 57(5), 2025-2042, <https://doi.org/10.1002/cjg2.20133>, 2014 (in
644 Chinese).

645 Densmore, A. L., Ellis, M.A., Yong, L., Zhou, R., Richardson, N.: Active tectonics of the Beichuan
646 and Pengguan faults at the eastern margin of the Tibetan Plateau. *Tectonics*, 26(4), TC4005,
647 <https://doi.org/10.1029/2006TC001987>, 2008.

648 Duvall, A., Kirby, E., Burbank, D.: Tectonic and lithologic controls on bedrock channel profiles and
649 processes in coastal California. *J. Geophys. Res. Earth Surface*, 109, F03002,
650 <https://doi.org/doi:10.1029/2003JF000086>, 2004.

651 Dietze, E., Maussion, F., Ahlborn, M., Diekmann, B., Hartmann, K., Henkel, K., Kasper, T., Lockot,
652 G., Opitz, S., Haberzettl, T.: Sediment transport processes across the Tibetan Plateau inferred
653 from robust grain-size end members in lake sediments. *Clim. Past*, 10, 91-106,
654 <https://doi.org/10.5194/cp-10-91-2014>, 2014.

655 Ding, H.R., Ma, G.W., Ni, S.J., Shi, Z.M., Zhao, G.H., Yan, L., Yan, Z.K.: Study on sediment
656 discharge increase caused by Wenchuan earthquake landslide and heavy rainfall in the upper
657 reaches of the Min River. *J. Sichuan Univ.*, 46(3), 49-55,
658 <https://doi.org/10.15961/j.jsuese.2014.03.006>, 2014 (in Chinese).

659 Egli, R.: Analysis of the field dependence of remanent magnetization curves. *J. Geophys. Res. Solid*
660 *Earth*, 108(B2), 1-26, <https://doi.org/10.1029/2002JB002023>, 2003.

661 Frings, R.M.: Downstream fining in large sand-bed rivers. *Earth Sci. Rev.*, 87, 39-60,
662 <https://doi.org/10.1016/j.earscirev.2007.10.001>, 2008.

663 Hovius, N., Meunier, P., Lin, C.W., Chen, H., Chen, Y.G., Dadson, S., Horng, M.J., Lines, M.:
664 Prolonged seismically induced erosion and the mass balance of a large earthquake. *Earth Planet.*
665 *Sci. Lett.*, 304(3-4), 347-355, <https://doi.org/10.1016/j.epsl.2011.02.005>, 2011.

666 Jiang, H., Zhang, J., Zhang, S., Zhong, N., Wan, S., Alsop, G.I., Xu, H., Guo, Q., Yan, Z.: Tectonic
667 and climatic impacts on environmental evolution in East Asia during the Palaeogene. *Geophys.*
668 *Res. Lett.*, 49, e2021GL096832, <https://doi.org/10.1029/2021GL096832>, 2022.

669 Jiang, H.C., Shevenell, A., Yu, S., Xu, H.Y., Mao, X.: Decadal- to centennial-scale East Asian
670 summer monsoon variability during the Medieval Climate Anomaly reconstructed from an

671 eastern Tibet lacustrine sequence. *J. Paleolimnology*, 54, 205-222,
672 <https://doi.org/10.1007/s10933-015-9847-1>, 2015.

673 Jiang, H.C., Mao, X., Xu, H.Y., Yang, H.L., Ma, X.L., Zhong, N., Li, Y.H.: Provenance and
674 earthquake signature of the last deglacial Xinmocun lacustrine sediments at Diexi, East Tibet.
675 *Geomorphology*, 204, 518-531, <https://doi.org/10.1016/j.geomorph.2013.08.032>, 2014.

676 Jiang, H.C., Zhong, N., Li, Y.H., Ma, X.L., Xu, H.Y., Shi, W., Zhang, S.Q., Nie, G.Z.: A continuous
677 13.3-ka record of seismogenic dust events in lacustrine sediments in the eastern Tibetan Plateau.
678 *Sci. Rep.*, 7:15686, <https://doi.org/10.1038/s41598-017-16027-8>, 2017.

679 Jiang, H.C., Zhong, N., Li, Y.H., Xu, H.Y., Yang, H.L., Peng, X.P.: Soft sediment deformation
680 structures in the Lixian lacustrine sediments, Eastern Tibetan Plateau and implications for
681 postglacial seismic activity. *Sediment. Geol.*, 344, 123-134,
682 <https://doi.org/10.1016/j.sedgeo.2016.06.011>, 2016.

683 Kirby, E., Whipple, K.X., Burchfiel, B.C., Tang, W.Q., Berger, G., Sun, Z.M., Chen, Z.L.:
684 Neotectonics of the Min Shan, China: implications for mechanisms driving quaternary
685 deformation along the eastern margin of the Tibetan Plateau. *GSA Bull.*, 112(3), 375-393,
686 [https://doi.org/10.1130/0016-7606\(2000\)112<375:NOTMSC>2.0.CO;2](https://doi.org/10.1130/0016-7606(2000)112<375:NOTMSC>2.0.CO;2), 2000.

687 Kirby, E., Reiners, P.W., Krol, M.A., Whipple, K.X., Hodges, K.V., Farley, K.A., Tang, W.Q., Chen,
688 Z.L.: Late Cenozoic evolution of the eastern margin of the Tibetan Plateau: inferences from
689 $^{40}\text{Ar}/^{39}\text{Ar}$ and U-Th/He thermochronology. *Tectonics*, 21(1), 1-20,
690 <https://doi.org/10.1029/2000TC001246>, 2002.

691 Kirby, E., Whipple, K. and Harkins, N.: Topography reveals seismic hazard. *Nat. Geosci.*, 1(8), 485-
692 487, <https://doi.org/10.1038/ngeo265>, 2008.

693 Kirby, E., Whipple, K.X., Tang, W.Q. and Chen, Z.L.: Distribution of active rock uplift along the
694 eastern margin of the Tibetan Plateau: Inferences from bedrock channel longitudinal profiles.
695 *J. Geophys. Res. Solid Earth*, 108(B4), 2217, <https://doi.org/doi:10.1029/2001JB000861>, 2003.

696 Kirkpatrick, H.M., Moon, S., Yin, A., Harrison, T.M.: Impact of fault damage on eastern Tibet
697 topography. *Geology*, 48, <https://doi.org/10.1029/2000TC00124610.1130/G48179.1>, 2020.

698 Li, G., Westa, A.J., Densmoreb, A.L., Jin, Z.D., Zhang, F., Wang, J., Clark, M., Hilton, R.G.:
699 Earthquakes drive focused denudation along a tectonically active mountain front. *Earth Planet.*
700 *Sci. Lett.*, 472, 253-265, <https://doi.org/10.1016/j.epsl.2017.04.040>, 2017.

701 Li, Y., Cao, S.Y., Zhou, R.J., Densmore, A.L., Ellis, M.: Late Cenozoic Minjiang incision rate and

702 its constraint on the uplift of the eastern margin of the Tibetan plateau. *Acta Geol. Sinica*, 79(1),
703 28-37, <https://doi.org/10.1007/s10409-004-0010-x10.3321/j.issn:0001-5717.2005.01.004>,
704 2005 (in Chinese).

705 Li, Y.H., Jiang, H.C., Xu, H.Y., Liang, L.J.: Analyses on the triggering factors of large quantities of
706 landslides in the upper reaches of the Minjiang River, Sichuan province. *Seism. Geol.*, 37(4),
707 1147-1161, <https://doi.org/10.3969/j.issn.0253-4967.2015.04.017>, 2015 (in Chinese).

708 Liang, S.M., Gan, W.J., Shen, C.Z., Xiao, G.R., Liu, J., Chen, W.T., Ding, X.G., Zhou, D.M.: Three-
709 dimensional velocity field of present-day crustal motion of the Tibetan Plateau derived from
710 GPS measurements. *J. Geophys. Res. Solid Earth*, 118(10), 1-11,
711 <https://doi.org/10.1002/2013JB010503>, 2013.

712 Liang, L.J. and Jiang, H.C.: Geochemical composition of the last deglacial lacustrine sediments in
713 East Tibet and implications for provenance, weathering and earthquake events. *Quat. Inter.*,
714 430, 41-51, <https://doi.org/10.1016/j.quaint.2015.07.037>, 2017.

715 Liu, M.: Research on the risk stone under wind loading with wind tunnel test in the Min River Valley.
716 Chengdu University of Technology, Sichuan, p. 10-38, 2014 (in Chinese).

717 Lin, M.B.: The huge Wenchuan earthquake and Longmen tectonic belt. *J. Chengdu Univ. Technol.*,
718 35(4), 366-370, <https://doi.org/10.3969/j.issn.1671-9727.2008.04.004>, 2008 (in Chinese).

719 Liu, W.M., Yang, S.L., Fang, X.M.: Loess recorded climatic change during the last glaciation on the
720 eastern Tibetan Plateau, western Sichuan. *J. Jilin Univ. Earth Sci. Edi.*, 43(3), 974-982,
721 <https://doi.org/http://ir.itpcas.ac.cn/handle/131C11/2852>, 2013 (in Chinese).

722 Liu, X.X., Wu, Y.Q., Jiang, Z.S., Zhan, W., Li, Q., Wen, W.X., Zhou, Z.Y.: Preseismic deformation
723 in the seismogenic zone of the Lushan Ms 7.0 earthquake detected by GPS observations. *Sci.*
724 *China, Earth Sci.*, 45(9), 1198-1207, <https://doi.org/10.1007/s11430-015-5128-0>, 2015.

725 Lu, H.Y., An, Z.S.: Comparison of grain-size distribution of Red Clay and Loess-paleosol deposits
726 in Chinese Loess Plateau. *Acta Sediment. Sinica*, 17(2), 226-232,
727 <https://doi.org/10.3969/j.issn.1000-0550.1999.02.011>, 1999.

728 Ma, K.M., Fu, B.J., Liu, S.L., Guan, W.B., Liu, G.H., Lu, Y.H., Anand, M.: Multiple-scale soil
729 moisture distribution and its implications to ecosystem restoration in an arid river valley, China.
730 *Land Degrad. Develop.*, 15(1), 75-85, <https://doi.org/10.1002/ldr.584>, 2004.

731 Ma, Y.W., Wang, G.Z., Hu, X.W.: Tectonic deformation of Pengguan complex as a nappe. *Acta Geol.*
732 *Sichuan*, 2, 110-114, <https://doi.org/CNKI:SUN:SCDB-0.1996-02-004>, 1996 (in Chinese).

733 Matmon, A., Bierman, P.R., Larsen, J., Southworth, S., Pavich, M., Caffee, M.: Temporally and

734 spatially uniform rates of erosion in the southern Appalachian Great Smoky Mountains.
735 *Geology*, 31, 155-158, [https://doi.org/10.1130/0091-7613\(2003\)0312.0.CO;2](https://doi.org/10.1130/0091-7613(2003)0312.0.CO;2), 2003a.

736 Matmon, A., Bierman, P.R., Larsen, J., Southworth, S., Pavich, M., Finkel, R., Caffee, M.: Erosion
737 of an ancient mountain range, the Great Smoky Mountains, North Carolina and Tennessee.
738 *Amer. J. Sci.*, 303, 817-855, <https://doi.org/10.2475/ajs.303.9.817>, 2003b.

739 McKinney, G.M., Sanders, J.E.: Principles of sedimentology. Wiley, New York, No. of pages 792,
740 1978.

741 Merritts, D., Vincent, K.R.: Geomorphic response of coastal streams to low, intermediate, and high
742 rates of uplift, Medocino triple junction region, northern California. *GSA Bull.*, 101, 1373-
743 1388, [https://doi.org/10.1130/0016-7606\(1989\)101<1373:GROCST>2.3.CO;2](https://doi.org/10.1130/0016-7606(1989)101<1373:GROCST>2.3.CO;2), 1989.

744 Middleton, G.V.: Hydraulic interpretation of sand size distributions. *J. Geol.*, 84(4), 405-426,
745 <https://doi.org/10.2307/30066059>, 1976.

746 Molnar, P., Anderson, R.S., Anderson, S.P.: Tectonics, fracturing of rock, and erosion. *J. Geophys.*
747 *Res. Earth Surface*, 112, F03014, <https://doi.org/10.1029/2005JF000433>, 2007.

748 Montgomery, D.R., Brandon, M. T.: Topographic controls on erosion rates in tectonically active
749 mountain ranges. *Earth Planet. Sci. Lett.*, 201(3), 481-489, [https://doi.org/10.1016/S0012-
750 821X\(0200725-2](https://doi.org/10.1016/S0012-821X(0200725-2), 2002.

751 Najman, Y.: The detrital record of orogenesis: A review of approaches and techniques used in the
752 Himalayan sedimentary basins. *Earth Sci. Rev.*, 74(1-2), 1-72,
753 <https://doi.org/10.1016/j.earscirev.2005.04.004>, 2006.

754 Nichols, K.K., Bierman, P.R., Caffee, M., Finkel, R., Larsen, J.: Cosmogenically enabled sediment
755 budgeting. *Geology*, 33(2), 133-136, <https://doi.org/10.1130/g21006.1>, 2005.

756 Olen, S.M., Bookhagen, B., Strecker, M.R.: Role of climate and vegetation density in modulating
757 denudation rates in the Himalaya. *Earth Planet. Sci. Lett.*, 445, 57-67,
758 <https://doi.org/10.1016/j.epsl.2016.03.047>, 2016.

759 Owen, L.A.: Tectonic geomorphology: a perspective. In: Shroder, J. (Editor in Chief), Owen, L.A.
760 (Ed.), *Treatise on Geomorphology*. Academic Press, San Diego, CA, vol. 5, Tectonic
761 Geomorphology, pp. 3-12, 2013.

762 Passega, R.: Texture as characteristic of clastic deposition. *Bull. Amer. Assoc. Petrol. Geol.*, 41,

763 1952-1984, <https://doi.org/10.1306/0BDA594E-16BD-11D7-8645000102C1865D>, 1957.

764 Paterson, G.A., Heslop, D.: New methods for unmixing sediment grain size data. *Geochem.*
765 *Geophys. Geosyst.*, 16(12), 4494-4506, <https://doi.org/info:doi/10.1002/2015GC006070>, 2015.

766 Perg, L.A., Anderson, R.S., Finkel, R.C.: Use of cosmogenic radionuclides as a sediment tracer in
767 the Santa Cruz littoral cell, California, USA. *Geology*, 31, 299-302,
768 [https://doi.org/10.1130/0091-](https://doi.org/10.1130/0091-7613(2003)0312.0.CO;2)
769 [7613\(2003\)0312.0.CO;2](https://doi.org/10.1130/0091-7613(2003)0312.0.CO;2), 2003.

770 Ren, J.J., Xu, X.W., Zhang, S.M., Yeats, R. S., Chen, J.W., Zhu, A.L., Liu, S.: Surface rupture of the
771 1933 Ms 7.5 Diexi earthquake in eastern Tibet: implications for seismogenic tectonics.
772 *Geophys. J. Inter.*, 212(3), 627-1644, <https://doi.org/10.1093/gji/ggx498>, 2018.

773 Riebe, C.S., Kirchner, J.W., Granger, D.E., Finkel, R.C.: Erosional equilibrium and disequilibrium
774 in the Sierra Nevada, inferred from cosmogenic ²⁶Al and ¹⁰Be in alluvial sediment. *Geology*,
775 28, 803-806, [https://doi.org/10.1130/0091-7613\(2000\)282.0.CO;2](https://doi.org/10.1130/0091-7613(2000)282.0.CO;2), 2000.

776 Riebe, S.R., Kirchner, J.W., Granger, D.E., Finkel, R.C.: Strong tectonic and weak climatic control
777 of long-term chemical weathering rates. *Geology*, 29, 511-514, [https://doi.org/10.1130/0091-](https://doi.org/10.1130/0091-7613(2001)0292.0.CO;2)
778 [7613\(2001\)0292.0.CO;2](https://doi.org/10.1130/0091-7613(2001)0292.0.CO;2), 2001.

779 Sahu, B. K.: Depositional mechanisms from the size analysis of clastic sediments. *J. Sediment. Res.*,
780 34, 73-83, <https://doi.org/10.1306/74D70FCE-2B21-11D7-8648000102C1865D>, 1964.

781 Schoenbohm, L.M., Whipple, K.X., Burchfiel, B.C., Chen, L.: Geomorphic constraints on surface
782 uplift, exhumation, and plateau growth in the Red River region, Yunnan Province, China. *GAS*
783 *Bull.*, 116, 895-909, <https://doi.org/10.1130/B25364.1>, 2004.

784 Schumm, S.A., Khan, H.R.: Experimental study of channel patterns. *Nature*, 233(5319), 407-9,
785 <https://doi.org/10.1038/233407a0>, 1971.

786 Schumm, S.A., Khan, H.R.: Experimental study of channel patterns. *GAS Bull.*, 83(6), 1755-1770,
787 <https://doi.org/10.1038/233407a0>[10.1130/0016-7606\(1972\)83\[1755:ESOCPI\]2.0.CO;2](https://doi.org/10.1130/0016-7606(1972)83[1755:ESOCPI]2.0.CO;2), 1972.

788 Selby, M.J.: A rock mass strength classification for geomorphic purposes, with tests from Antarctica
789 and New Zealand: *Zeitschrift für Geomorphologie*, v. 24, p. 31–51, 1980.

790 Shen, Y.Q., Guo, C.B., Wu, R.A., Ren, S.S., Su, F.R., Zhang, T.: Analysis on the development
791 characteristics and engineering geomechanical properties of the Songpan loess, western

792 Sichuan province, China. *J. Geomech.*, 23(5), 131-142,
793 <https://doi.org/CNKI:SUN:DZLX.0.2017-05-045><https://doi.org/10.3969/j.issn.1006->
794 [6616.2017.05.013](https://doi.org/10.3969/j.issn.1006-6616.2017.05.013), 2017 (in Chinese).

795 Shi, W., Jiang, H.C., Mao, X., Xu, H.Y.: Pollen record of climate change during the last deglaciation
796 from the eastern Tibetan Plateau. *PLOS ONE*, 15(5), e0232803,
797 <https://doi.org/10.1371/journal.pone.0232803>, 2020.

798 Shi, W., Jiang, H.C., Alsop, G.I., Wu, G.: A Continuous 13.3-Ka paleoseismic record constrains
799 major earthquake recurrence in the Longmen Shan collision zone. *Front. Earth Sci.*, 10:838299,
800 <https://doi.org/10.3389/feart.2022.838299>, 2022.

801 Singh, M., Singh, I.B., Müller, G.: Sediment characteristics and transportation dynamics of the
802 Ganga River. *Geomorphology*, 86(1/2), 144-175,
803 <https://doi.org/10.1016/j.geomorph.2006.08.011>, 2007.

804 Snyder, N., Whipple, K., Tucker, G., Merritts, D.: Landscape response to tectonic forcing: digital
805 elevation model analysis of stream profiles in the Mendocino triple junction region, northern
806 California. *GAS Bull.*, 112, 1250-1263, [https://doi.org/10.1130/0016-](https://doi.org/10.1130/0016-7606(2000)112<1250:LRTTFD>2.0.CO;2)
807 [7606\(2000\)112<1250:LRTTFD>2.0.CO;2](https://doi.org/10.1130/0016-7606(2000)112<1250:LRTTFD>2.0.CO;2)[https://doi.org/10.1130/0016-](https://doi.org/10.1130/0016-7606(2000)1122-0.CO;2)
808 [7606\(2000\)1122-0.CO;2](https://doi.org/10.1130/0016-7606(2000)1122-0.CO;2), 2000.

809 Snyder, N.P. and Whipple, K.X.: Importance of a stochastic distribution of floods and erosion
810 thresholds in the bedrock river incision problem. *J. Geophys. Res. Solid Earth*, 108, 2117,
811 <https://doi.org/10.1029/2001JB001655>, 2003.

812 Stock, J. D., Dietrich, W. E.: Valley incision by debris flows: evidence of a topographic signature.
813 *Water Resour. Res.*, 39(4), ESG 1-1, <https://doi.org/10.1029/2001WR001057>, 2003.

814 Stokes, M., Mather, A.E., Belfoul, A., Farik, F.: Active and passive tectonic controls for transverse
815 drainage and river gorge development in a collisional mountain belt (Dades Gorges, High Atlas
816 Mountains, Morocco). *Geomorphology*, 102(1), 2-20,
817 <https://doi.org/10.1016/j.geomorph.2007.06.015>, 2008.

818 Stokes, M., Mather, A.E., Harvey, A.M.: Quantification of river-capture-induced base-level changes
819 and landscape development, Sorbas Basin, SE Spain. *Geol. Soc. London Spec. Publ.*, 191(1),
820 23-35, <https://doi.org/10.1144/GSL.SP.2002.191.01.03>, 2002.

821 Sun, D.H., Bloemendal, J., Rea, D.K., An, Z.S., Vandenberghe, J., Lu, H.Y., Sun, R.X., Liu, T.S.:

822 Bimodal grain-size distribution of Chinese loess, and its palaeoclimatic implications. *Catena*,
823 55(3), 325-340, [https://doi.org/10.1016/S0341-8162\(0300109-7](https://doi.org/10.1016/S0341-8162(0300109-7), 2004.

824 Sun, D.H., Bloemendal, J., Rea, D.K., Vandenberghe, J., Jiang, F.C., An, Z.S., Su, R.X.: Grain-size
825 distribution function of polymodal sediments in hydraulic and aeolian environments, and
826 numerical partitioning of the sedimentary components. *Sediment. Geol.*, 152(3-4), 263-277,
827 [https://doi.org/10.1016/S0037-0738\(0200082-9](https://doi.org/10.1016/S0037-0738(0200082-9), 2002.

828 Sun, J.M, Li, S.H., Muhs, D. R., Li, B.: Loess sedimentation in Tibet: provenance, processes, and
829 link with Quaternary glaciations, *Quat. Sci. Rev.*, 26(17-18), 2265-2280,
830 <https://doi.org/10.1016/j.quascirev.2007.05.003>, 2007.

831 Tan, X.B., Liu, Y.D., Lee, Y.H., Lu, R.Q., Xu, X.W., Suppe, J., Shi, F., Xu, C.: Parallelism between
832 the maximum exhumation belt and the Moho ramp along the eastern Tibetan Plateau margin:
833 Coincidence or consequence?. *Earth Planet. Sci. Lett.*, 507, 73-84,
834 <https://doi.org/10.1016/j.epsl.2018.12.001>, 2019.

835 Tsoar, H., Pye, K.: Dust transport and the question of desert loess formation. *Sedimentology*, 34(1),
836 139-153, <https://doi.org/10.1111/j.1365-3091.1987.tb00566.x>, 1987.

837 Vandenberghe, J.: Grain size of fine-grained windblown sediment: a powerful proxy for process
838 identification. *Earth Sci. Rev.*, 121, 18-30, <https://doi.org/10.1016/j.earscirev.2013.03.001>,
839 2013.

840 Wang, J., Jin, Z.D., Hilton, R.G., Zhang, F., Densmore, A.L., Li, G., West A.J.: Controls on fluvial
841 evacuation of sediment from earthquake-triggered landslides. *Geology*, 43(2), 115-118,
842 <https://doi.org/10.1130/G36157.1>, 2015.

843 Wang, P., Zhang, B., Qiu, W.L., Wang, J.C.: Soft-sediment deformation structures from the Diexi
844 paleo-dammed lakes in the upper reaches of the Minjiang River, east Tibet. *J. Asian Earth Sci.*,
845 40(4), 865-872, <https://doi.org/10.1016/j.jseaes.2010.04.006>, 2011.

846 Wang, P., Scherler, D., Liu-Zeng, J., Mey, J., Avouac, J.P., Zhang, Y., Shi, D.: Tectonic control of
847 Yarlung Tsangpo gorge revealed by a buried canyon in southern Tibet. *Science*, 346, 978-981,
848 <https://doi.org/10.1126/science.1259041>, 2014.

849 Wang, W., Godard, V., Liu-Zeng, J., Scherler, D., Xu, C., Zhang, J.Y., Xie, K.J., Bellier, O.,
850 Ansberque, C., Sigoyer, J., Team, A.: Perturbation of fluvial sediment fluxes following the

851 2008 Wenchuan earthquake. *Earth Surf. Process Land.*, 42(15), 2611-2622,
852 <https://doi.org/10.1002/esp.4210>, 2017.

853 Wang, W., Godard, V., Liu-Zeng, J., Zhang, J.Y., Li, Z.G., Xu, S., Yao, W.Q., Yuan, Z.D., Aumaître,
854 G., Bourlès, D.L., Keddadouche, K.: Tectonic controls on surface erosion rates in the Longmen
855 Shan, eastern Tibet. *Tectonics*, 40(3), <https://doi.org/10.1029/2020TC006445>, 2021.

856 Wang, X.G., Li, C.Y., Lu, L.X., Dong, J.B.: Analysis of the late Quaternary activity along the
857 Wenchuan-Maoxian fault-middle of the back- range fault at the Longmen Shan fault zone.
858 *Seism. Geol.*, 39(3), 572-586, <https://doi.org/10.3969/j.issn.0253-4967.2017.03.010>, 2017.

859 Weltje, G.L.: End-member modeling of compositional data: Numerical-statistical algorithms for
860 solving the explicit mixing problem. *Mathemat. Geol.*, 29(4), 503-549,
861 <https://doi.org/10.1007/BF02775085>, 1997.

862 Wei, X.T., Jiang, H.C., Xu, H.Y., Fan, J.W., Shi, W., Guo, Q.Q., Zhang, S.Q.: Response of
863 sedimentary and pollen records to the 1933 Diexi earthquake on the eastern Tibetan Plateau.
864 *Ecol. Indicators*, 129, 107887, <https://doi.org/10.1016/j.ecolind.2021.107887>, 2021.

865 Whipple, K.X.: Bedrock rivers and the geomorphology of active orogens. *Ann. Rev. Earth Planet.*
866 *Sci.*, 32, 151-185, <https://doi.org/10.1146/annurev.earth.32.101802.120356>, 2004.

867 Whittaker, A.C., Attalw, M., Allenn, P.A.: Characterising the origin, nature and fate of sediment
868 exported from catchments perturbed by active tectonics. *Basin Res.*, 22, 809-828,
869 <https://doi.org/10.1111/j.1365-2117.2009.00447.x>, 2010.

870 Whittaker, A. C., Cowie, P.A., Attal, M., Tucker, G. E., Roberts, G.P.: Contrasting transient and
871 steady-state rivers crossing active normal faults: new field observations from the central
872 Apennines, Italy. *Basin Res.*, 19(4), 529-556, <https://doi.org/10.1111/j.1365-2117.2007.00337>,
873 2007.

874 Wu, H.B., Liu, X.M., Lv, B., Ma, M.M., Ji, J.P., Wang, W.Y., Zhang, Y.Y., Hou, J.L.: Aeolian origin
875 of the Twelve Apostles section, in Australia. *Quat. Sci.*, 37(1), 82-96,
876 <https://doi.org/10.11928/j.issn.1001-7410.2017.01.08>, 2017 (in Chinese).

877 Wobus, C., Heimsath, A., Whipple, K. Hodges, K.: Active out-of-sequence thrust faulting in the
878 central Nepalese Himalaya. *Nature*, 434, 1008-1011, <https://doi.org/10.1038/nature03499>,
879 2005.

880 Wobus, C.W., Tucker, G.E., and Anderson, R.S.: Does climate change create distinctive patterns of
881 landscape incision? *J. Geophys. Res.*, 115, F04008, <https://doi.org/10.1029/2009JF001562>,
882 2010.

883 Xu, C., Xu, X.W., Dai, F.C., Xiao, J.Z., Tan, X.B., Yuan, R.M.: Landslides hazard mapping using
884 GIS and weight of evidence model in Qingshui River watershed of 2008 Wenchuan earthquake
885 struck region. *J. Earth Sci.*, 23(1), 97-120, [https://doi.org/10.1007/s12583-012-0236-](https://doi.org/10.1007/s12583-012-0236-7)
886 [7https://doi.org/CNKI:SUN:ZDDY.0.2012-01-010](https://doi.org/CNKI:SUN:ZDDY.0.2012-01-010), 2012.

887 Xu, C., Xu, X.W., Yao, X., Dai, F.C.: Three, nearly complete inventories of landslides triggered by
888 the May 12, 2008 Wenchuan Mw 7.9 earthquake of China and their spatial distribution
889 statistical analysis. *Landslides*, 11(3), 441-461, <https://doi.org/10.1007/s10346-013-0404-6>,
890 2014.

891 Xu, H.Y., Jiang, H.C., Liu, K., Zhong, N.: Potential pollen evidence for the 1933 M7.5 Diexi
892 earthquake and implications for post-seismic landscape recovery. *Enviro. Res. Lett.*, 15:094043,
893 <https://doi.org/10.1088/1748-9326/ab9af6>, 2020.

894 Xu, H.Y., Jiang, H.C., Yu, S., Yang, H.L., Chen, J.: OSL and pollen concentrate ¹⁴C dating of
895 dammed lake sediments at Maoxian, east Tibet, and implications for two historical earthquakes
896 in AD 638 and 952. *Quat. Inter.*, 371, 290-299, <https://doi.org/10.1016/j.quaint.2014.09.045>,
897 2015.

898 Zhang, F., Jin, Z.D., West, A.J., An, Z.S., Hilton, R.G., Wang, J., Li, G., Densmore, A.L., Yu, J.M.,
899 Qiang, X.K., Sun, Y.B., Li, L.B., Gou, L.F., Xu, Y., Xu, X.W., Liu, X.X., Pan, Y.H., You, C.F.:
900 Monsoonal control on a delayed response of sedimentation to the 2008 Wenchuan earthquake.
901 *Sci. Adv.*, 5(6), eaav7110, <https://doi.org/10.1126/sciadv.aav7110>, 2019.

902 ~~Zhang, P., Zhou, Z.Y., Xu, C.H., Zhang, Q.L.: Geochemistry of Pengguan complex in the~~
903 ~~Longmenshan region, western Sichuan Province, SW China: petrogenesis and tectonic~~
904 ~~implications. *Geotecton. Metallog.*, 32(1), 105-116, 2008 (in Chinese).~~

905 Zhang, P.Z., Deng, Q.D., Zhang, M.G., Ma, J., Gan, W.J., Wei, M., Mao, F.Y., Wang, Q.: Active
906 tectonic blocks and strong earthquakes in the continent of China. *Sci. China*, 46, 13-24,
907 <https://doi.org/10.3969/j.issn.1674-7313.2003.z2.002><https://doi.org/10.1360/03dz0002>, 2003.

908 ~~Zhang, P.Z., Zhou, Z.Y., Xu, C.H., Zhang, Q.L.: Geochemistry of Pengguan complex in the~~

909 [Longmenshan region, western Sichuan Province, SW China: petrogenesis and tectonic](#)
910 [implications. Geotecton. Metallog., 32\(1\), 105-116, \[1552.2008.01.014, 2008 \\(in Chinese\\).\]\(https://doi.org/10.3969/j.issn.1001-
911 <a href=\)](#)

912 Zhang, S.Q., Jiang, H.C., Fan, J.W., Xu, H.Y., Shi, W., Guo, Q.Q. and Wei, X.T.: Accumulation of
913 a last deglacial gravel layer at Diexi, eastern Tibetan Plateau and its possible seismic
914 significance. *Front. Earth Sci.*, 9:797732, <https://doi.org/10.3389/feart.2021.797732>, 2021.

915 Zhang, Y.Q., Yang, N., Meng, H.: Deep-incised valleys along the Minjiang river upstream and their
916 responses to the uplift of the West Sichuan Plateau, China. *J. Chengdu Univ. Technol.*, 32(4),
917 331-339, [https://doi.org/10.3969/j.issn.1671-](https://doi.org/10.3969/j.issn.1671-9727.2005.04.001)
918 [9727.2005.04.001](https://doi.org/1671-9727.2005.04.001)<https://doi.org/CNKI:SUN:CDLG.0.2005-04-000>, 2005 (in Chinese).

919 Zhou R.J., Li, Y., Densmore, A.L., Ellis, M.A., He, Y.L., Wang, F.L., Li, X.G.: Active tectonics of
920 the eastern margin of the Tibet Plateau. *J. Mineral. Petrol.*, 26(2),40-51,
921 <https://doi.org/10.3969/j.issn.1001-6872.2006.02.007>, 2006 (in Chinese).

922 Zhou, R.J., Pu, X.H., He, Y.L., Li, X.G., Ge, T.Y.: Recent activity of Minjiang fault zone, uplift of
923 Minshan Block and their relationship with seismicity of Sichuan. *Seism. Geol.*, 22(3),285-294,
924 <https://doi.org/CNKI:SUN:DZDZ.0.2000-03-009>, 2000 (in Chinese).

925 Zhou, R.Y., Wen, X.Y., Lu, L., Li, Y.X., Huang, C.M.: Holocene paleosols and paleoclimate for the
926 arid upper Minjiang River valley in the eastern Tibetan Plateau. *Catena*, 206, 105555,
927 <https://doi.org/10.1016/j.catena.2021.105555>, 2021.

928 Zhong, N., Jiang, H.C., Li, H.B., Xu, H.Y., Shi, W., Zhang, S.Q., Wei, X.T.: Last Deglacial Soft-
929 Sediment Deformation at Shawan on the Eastern Tibetan Plateau and Implications for
930 Deformation Processes and Seismic Magnitudes. *Acta Geol. Sinica*, 93(2), 430-450,
931 <https://doi.org/10.1111/1755-6724.13773>, 2019.

932 Zhong, N., Song, X.S., Xu, H.Y., Jiang, H.C.: Influence of a tectonically active mountain belt on its
933 foreland basin: Evidence from detrital zircon dating of bedrocks and sediments from the eastern
934 Tibetan Plateau and Sichuan Basin, SW China. *J. Asian Earth Sci.*, 146, 251-264,
935 <https://doi.org/10.1016/j.jseaes.2017.05.035>, 2017.

936 Zondervan, J., Stokes, M., Boulton, S., Telfer, M., Mather, A.: Rock strength and structural controls
937 on fluvial erodibility: Implications for drainage divide mobility in a collisional mountain belt.

